

The strength of the meridional overturning circulation of the stratosphere

Marianna Linz^{1*}†, R. Alan Plumb², Edwin P. Gerber³, Florian J. Haenel⁴, Gabriele Stiller⁴, Douglas E. Kinnison⁵, Alison Ming⁶ and Jessica L. Neu⁷

The distribution of gases such as ozone and water vapour in the stratosphere—which affect surface climate—is influenced by the meridional overturning of mass in the stratosphere, the Brewer–Dobson circulation. However, observation-based estimates of the global strength of this circulation are difficult to obtain. Here we present two calculations of the mean strength of the meridional overturning of the stratosphere. We analyse satellite data that document the global diabatic circulation between 2007–2011, and compare these to three reanalysis data sets and to simulations with a state-of-the-art chemistry–climate model. Using measurements of sulfur hexafluoride (SF₆) and nitrous oxide, we calculate the global mean diabatic overturning mass flux throughout the stratosphere. In the lower stratosphere, these two estimates agree, and at a potential temperature level of 460 K (about 20 km or 60 hPa in tropics) the global circulation strength is $6.3\text{--}7.6 \times 10^9 \text{ kg s}^{-1}$. Higher in the atmosphere, only the SF₆-based estimate is available, and it diverges from the reanalysis data and simulations. Interpretation of the SF₆-data-based estimate is limited because of a mesospheric sink of SF₆; however, the reanalyses also differ substantially from each other. We conclude that the uncertainty in the mean meridional overturning circulation strength at upper levels of the stratosphere amounts to at least 100%.

Previous calculations of the strength of the stratospheric circulation from data have relied on indirect measures. Observational estimates of the strength of the overturning have been limited to qualitative descriptions based on tracer distributions^{1–4} or quantitative measures of limited regions, such as the vertical velocity over a narrow range in the tropics^{5–7}. Free-running climate models vary widely in stratospheric circulation metrics, including the tropical upwelling mass flux at 10 hPa and 70 hPa, although the multimodel mean is relatively close to some reanalysis products⁸. Reanalyses, meanwhile, differ substantially in their mean tropical upwelling velocity, with the magnitude of the mismatch depending on how it is computed⁹. Here we consider the diabatic circulation of the stratosphere; because the stratosphere is stratified, vertical motion moves air across potential temperature surfaces and thus must be associated with warming/cooling in the ascending/descending branches. Hence, the net meridional overturning of mass is tightly linked to diabatic processes. We use potential temperature as our vertical coordinate, and the meridional overturning becomes explicitly the diabatic circulation in this framework.

The diabatic circulation has been shown to be related to the idealized tracer ‘age of air’^{10,11}, which is a measure of how long an air parcel has spent in the stratosphere¹². The difference between the age of the air that is upwelling and downwelling through an isentropic surface is inversely proportional to the strength of the diabatic circulation through that surface, in steady state and neglecting diabatic diffusion.

In this paper, we apply this age difference theory to calculate the mean magnitude and vertical structure of the global overturning

circulation of the stratosphere using observations of sulfur hexafluoride (SF₆) and nitrous oxide (N₂O). We demonstrate the validity of the theory and explore limitations of the tracer data with a coupled chemistry–climate model. We calculate the global overturning directly from the diabatic vertical velocity from three reanalyses to compare with the data and model results. Information on the data products, model, and reanalyses is given in Table 1.

Age of air observations and model

A trace gas that is linearly increasing in time in the troposphere and has no stratospheric sinks can be converted to age following age of air theory¹². Carbon dioxide (CO₂) and SF₆ are both approximately linearly increasing in the troposphere and have minimal sinks in the stratosphere. We use age derived from SF₆ measurements (henceforth SF₆-age) from the Michelson Interferometer for Passive Atmospheric Sounding (MIPAS) on Envisat⁴. We interpolate SF₆-age onto isentropic surfaces using simultaneously retrieved pressure and temperature from MIPAS^{13,14}. The resulting SF₆-age on the 500 K surface is shown in Fig. 1a. Age is young in the tropics, older in the extratropics, and oldest at the winter poles, consistent with the pattern of upwelling in the tropics and the majority of downwelling in the winter polar region. The SF₆-age at high latitudes in wintertime is older than observations of age based on CO₂ measurements^{15,16}. SF₆ is not conserved in the mesosphere, and its sink will result in a high bias in SF₆-age in areas with mesospheric influence¹⁷, such as the poles and the upper stratosphere.

To explore the limitations of using SF₆-age, we compare SF₆-age to ideal age of air in a coupled chemistry–climate model, the

¹Massachusetts Institute of Technology—Woods Hole Oceanographic Institution Joint Program in Physical Oceanography, Massachusetts Institute of Technology, Cambridge, Massachusetts 02139, USA. ²Department of Earth, Atmospheric and Planetary Sciences, Massachusetts Institute of Technology, Cambridge, Massachusetts 02139, USA. ³Courant Institute of Mathematical Sciences, New York University, New York, New York 10012, USA. ⁴Karlsruhe Institute of Technology, Institute of Meteorology and Climate Research, Karlsruhe 76021, Germany. ⁵Atmospheric Chemistry Observations and Modeling Laboratory, National Center for Atmospheric Research, Boulder, Colorado 80307, USA. ⁶Department of Applied Mathematics and Theoretical Physics, University of Cambridge, Cambridge CB3 0WA, UK. ⁷Jet Propulsion Laboratory, California Institute of Technology, Pasadena, California 91109, USA.

†Present address: Department of Atmospheric and Oceanic Sciences, University of California, Los Angeles, California 90095, USA.

*e-mail: mlinz@atmos.ucla.edu

Table 1 | Data, reanalyses, and model output used in this study.

Data source	Variables	Resolution	Time period	Reference(s)
MIPAS	Age from SF ₆ ; temperature; pressure	Zonal mean, 10° latitude, 41 levels from 8 km to 54 km	2002–2012	4,13,14
GOZCARDS	N ₂ O	Zonal mean, 10° latitude, 15 pressure levels from 100 to 0.46 hPa	2004–2014	29,30
EPA Climate Indicators	Tropospheric N ₂ O	<i>In situ</i> surface	1980–2014	46
WACCM	SW; LW; temperature; ideal age; SF ₆	2.5° longitude, 1.875° latitude, 31 pressure levels from 193 hPa to 0.3 hPa	1979–2014	18,19
JRA 55	SW; LW; temperature	1.25° × 1.25°, 16 pressure levels from 225 hPa to 1 hPa	1979–2014	35
MERRA	Total dT/dt; temperature	1.25° × 1.25°, 17 pressure levels from 200 hPa to 0.5 hPa	1979–2014	34
ERA-Interim	SW; LW; temperature	1° × 1°, 26 pressure levels from 150 hPa to 0.5 hPa	1979–2014	36

SW is the shortwave radiation and LW is the longwave radiation.

Community Earth System Model 1 Whole Atmosphere Community Climate Model (WACCM). This fully coupled state-of-the-art interactive chemistry–climate model^{18,19} includes the physical parameterizations and finite-volume dynamical core²⁰ from the Community Atmosphere Model, version 4 (ref. 21). The model domain extends from the Earth's surface to the lower thermosphere (140 km). The WACCM simulations are based on the Chemistry–Climate Model Initiative REF-C1 scenario²². WACCM models only one of the two sinks of SF₆ in the mesosphere; photolysis at Lyman-alpha wavelengths is included, but associative electron attachment, recently shown to be the dominant loss mechanism for SF₆ below 105 km (refs 23,24), is not. The impact of the mesospheric sink of SF₆ on stratospheric SF₆ will be determined by the strength of the dynamical coupling between the stratosphere and the mesosphere. We calculate SF₆-age using the same methods as were used to calculate MIPAS SF₆-age¹ (for details see Methods). Although WACCM is missing the dominant SF₆ loss mechanism, the difference between SF₆-age and ideal age will qualitatively illustrate the sense and location of any bias introduced by using SF₆ as an age tracer.

Age on the 500 K surface between 2002 and 2012 is shown for WACCM SF₆-age in Fig. 1c, and for WACCM ideal age of air in Fig. 1d. The agreement between ideal age and SF₆-age on the 500 K surface suggests that SF₆-age is a good proxy for ideal age at this level in the model. The temporal correlation at each latitude on the 500 K surface is high ($r = 0.93$), and only at the poles is SF₆-age older than ideal age by up to half a year. Where there is more mesospheric influence the correlation is weaker and no longer one to one: higher in the stratosphere and at the highest latitudes ($r = 0.52$ and age has only 35% of the magnitude of variations of SF₆-age at 1,200 K, 85° N). Since WACCM is missing the dominant sink of SF₆, these differences represent a lower bound on the bias from using SF₆-age as a proxy for ideal age.

The difference between the MIPAS SF₆-age and WACCM SF₆-age is substantial. MIPAS SF₆-age has been shown to be consistently older than *in situ* CO₂ and SF₆ age observations, although typically within error estimates¹⁴ (see Supplementary Information). In the tropics, these known high biases are almost the same as the difference between WACCM SF₆-age and MIPAS SF₆-age. In the polar region, a similar amount of bias exists at low levels, and at upper levels there are no *in situ* measurements for comparison. In WACCM, the dynamical coupling of the stratosphere and mesosphere has been shown in certain events to be too weak^{25,26}, and in another case to be accurate¹⁶, and so the reliability of the model's transport of mesospheric air into the stratosphere is unclear.

Given the potential biases of SF₆-age and the MIPAS data, other age tracers are desirable to corroborate the circulation strength

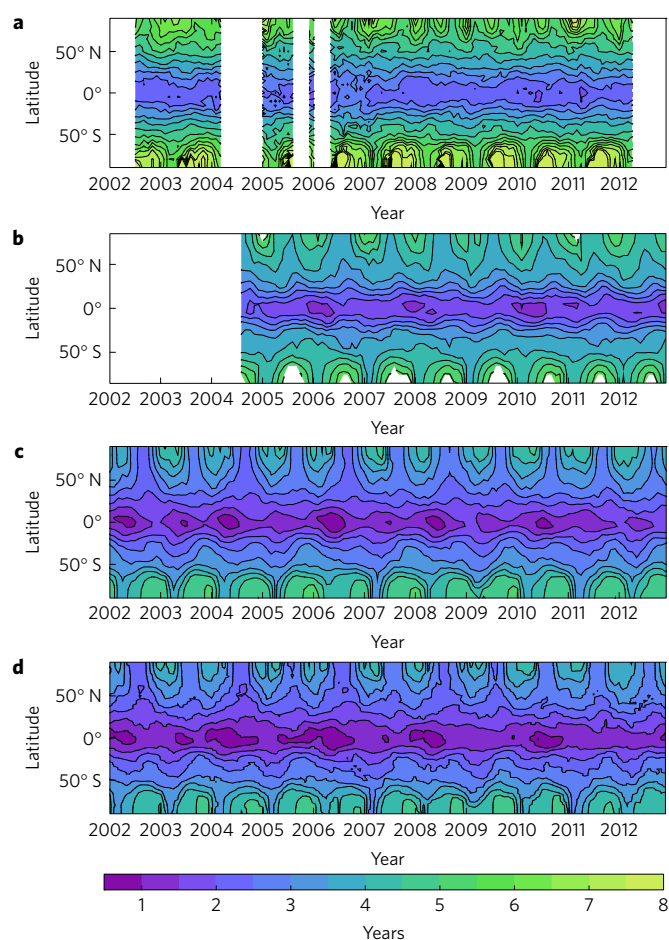


Figure 1 | Age of air on the 500 K surface. a–d, The different panels show age calculated from SF₆ from MIPAS (a), N₂O from GOZCARDS (b), SF₆ from WACCM (c) and WACCM ideal age tracer (d). Contours are every half year, and the ages in the Southern Hemisphere winter for MIPAS get above 8 years old.

calculations from SF₆-age. CO₂ is currently not retrieved from satellites with enough accuracy and spatial coverage to calculate age of air differences²⁷. Instead, we determine age from N₂O, which demonstrates a compact relationship with age, like other long-lived stratospheric tracers²⁸. We use a relationship between age of air and N₂O calculated empirically from balloon and aircraft

measurements²⁹, accounting for the linear growth in tropospheric N₂O. Following the procedure outlined in the Methods, we calculate age of air from the Global Ozone Chemistry And Related trace gas Data records for the Stratosphere (GOZCARDS) N₂O data for 2004–2013³⁰. Because of the range of tracer values over which the empirical relationship holds, global coverage exists for a small range in potential temperature (about 450 K–500 K, Supplementary Fig. 8). An additional empirical relationship³¹ is explored in the Supplementary Information.

The age on the 500 K surface calculated from its empirical relationship with N₂O is shown in Fig. 1b. The Southern Hemisphere winter polar coverage is limited because N₂O concentrations are below 50 ppb, the lower limit of the empirical fit. Age from the N₂O data is generally younger than MIPAS SF₆-age, although older than age from WACCM. The temporal correlation of MIPAS SF₆-age and N₂O-age at every latitude on the 500 K surface is around $r = 0.5$, except in the Northern Hemisphere mid-latitudes, where the correlation is not significant.

Age difference and the diabatic circulation

In steady state, the diabatic circulation (\mathcal{M}) through an isentropic surface wholly within the stratosphere can be calculated as the ratio of the mass above the surface (M) to the difference in the mass-flux-weighted age of downwelling and upwelling air on the surface ($\Delta\Gamma$, or age difference)¹¹.

$$\mathcal{M} = M / \Delta\Gamma \quad (1)$$

\mathcal{M} is the total mass flux upwelling (or downwelling, as in steady state these must be equal) through the isentropic surface. (See Figure 1 of ref. 11 for a diagram.) Intuitively this reflects the idea of a residence time; the age difference is how long the air spent above the surface, and it is equal to the ratio of the mass above the surface to the mass flux passing through that surface.

The real world is not in steady state, and so averaging is necessary for this theory to apply. A minimum of one year of averaging was necessary for the theory to hold in an idealized model¹¹. As the MIPAS instrument has five years of continuous data, the longest average possible for this study is five years. To test the validity of applying the steady-state theory to five-year averages, we have calculated the 2007–2011 averages of ideal age difference and the ratio of the total mass above each isentrope to the mass flux through that isentrope from WACCM output. These are shown in the blue lines (solid and dotted, respectively) in Fig. 2. The total overturning strength is calculated from the potential temperature tendency, θ , which is the total all-sky radiative heating rate interpolated onto isentropic surfaces. The upwelling and downwelling regions are defined where θ is instantaneously positive or negative, and the mass fluxes through these regions are averaged to obtain the total overturning mass flux, \mathcal{M} . If the age difference theory held exactly, the two blue lines in Fig. 2 would be identical. In the upper stratosphere, these two calculations agree closely; in the lower stratosphere, the ratio of the mass to the mass flux is greater than the ideal age $\Delta\Gamma$. This behaviour is consistent with the neglect of diabatic diffusion, which is greater in the lower stratosphere³². Using area weighting of ideal age, since mass-flux weighting is not possible with data, results in about a 10% low bias of $\Delta\Gamma$ compared to the mass-flux weighting shown here.

We calculate the five-year average (2007–2011) of the difference in area-weighted age of air in the regions poleward and equatorward of 35° from the SF₆-age from both MIPAS and WACCM, and from the N₂O-age. (See Supplementary Information and Supplementary Fig. 1 for a discussion of this latitudinal extent.) The results of this are shown in Fig. 2. The MIPAS SF₆-age $\Delta\Gamma$ is different from the other estimates except around 450 K. At 400 K, it is smaller, in part because of older tropical air at that level (see Supplementary Fig. 10). Above 500 K, MIPAS SF₆ $\Delta\Gamma$ is much greater than the model $\Delta\Gamma$ using either ideal age or SF₆-age. Age difference for N₂O

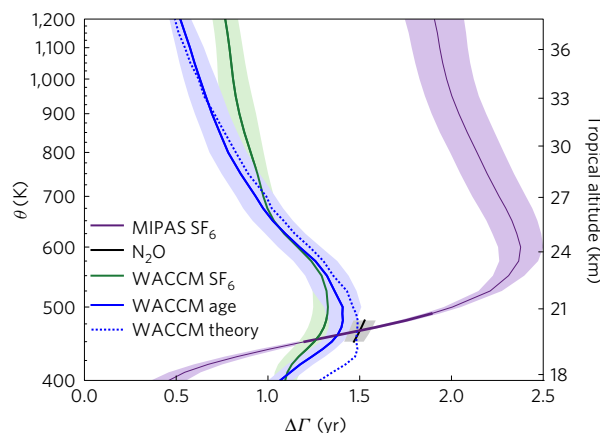


Figure 2 | The average age difference between downwelling and upwelling age of air on each isentrope between 2007–2011. $\Delta\Gamma$ is plotted in solid lines: MIPAS SF₆-age in purple, GOZCARDS N₂O-age in black, WACCM SF₆-age in green, and WACCM ideal age of air in the blue. The blue dotted line shows the ratio of the total mass above each isentrope to the mass flux through the isentrope (M/\mathcal{M}) from WACCM. The shading shows one standard deviation of the five annual averages that are averaged to get the mean. The mean height of each isentrope in the tropics (calculated from MIPAS pressure and temperature) is on the right y-axis. Where the line for the MIPAS SF₆-age difference is thinner, we believe there is a bias in either the data or the SF₆ to age conversion (see discussion in Supplementary Information).

is calculated only where data is available over the entire surface at almost all times, 450–480 K (extended in Supplementary Fig. 9). In this limited range, the age difference from N₂O-age is greater than the age difference from WACCM and agrees with the age difference calculated from MIPAS SF₆-age.

To gain insight into the role of the mesospheric sink, we compare the ideal age $\Delta\Gamma$ with SF₆-age $\Delta\Gamma$ in WACCM. The ideal age $\Delta\Gamma$ is the mass-flux-weighted age difference between upwelling and downwelling regions, and the SF₆-age $\Delta\Gamma$ from WACCM is calculated in the same way as the MIPAS SF₆-age $\Delta\Gamma$. Because of the area weighting, we expect the SF₆-age $\Delta\Gamma$ to be 10% lower than the ideal age $\Delta\Gamma$. This is true from 450–550 K, but above that, the SF₆-age $\Delta\Gamma$ is either equal to or greater than the ideal age $\Delta\Gamma$, and at 1,200 K SF₆-age $\Delta\Gamma$ is 50% greater. Since WACCM does not include the dominant sink of SF₆ for the mesosphere, we cannot estimate an upper bound on the true bias.

All three calculations of $\Delta\Gamma$ from the model as well as the $\Delta\Gamma$ from MIPAS SF₆-age show a peak in the middle stratosphere. This peak indicates a relative minimum of the diabatic velocity at that level, and so this provides evidence that there are indeed two branches of the circulation³³.

Circulation from reanalyses, model, and age

Figure 3 shows the total overturning circulation strength calculated using the ratio of the total mass above the isentrope to $\Delta\Gamma$ for the MIPAS SF₆-age and the N₂O-age. Total mass is determined from the simultaneously retrieved pressure in the former case and from pressure from the Modern Era Retrospective analysis for Research and Applications (MERRA³⁴) for N₂O. Also shown is the directly calculated overturning circulation strength from the three reanalysis products MERRA, Japanese 55-year Reanalysis (JRA 55 (ref. 35)) and the ECMWF Reanalysis Interim (ERA-Interim³⁶), and from WACCM. The total overturning strength is calculated from the potential temperature tendency, θ , from the total diabatic heating rates from JRA 55 and ERA-Interim forecast products and from total temperature tendency provided by MERRA, and then following the same procedure as above for WACCM.

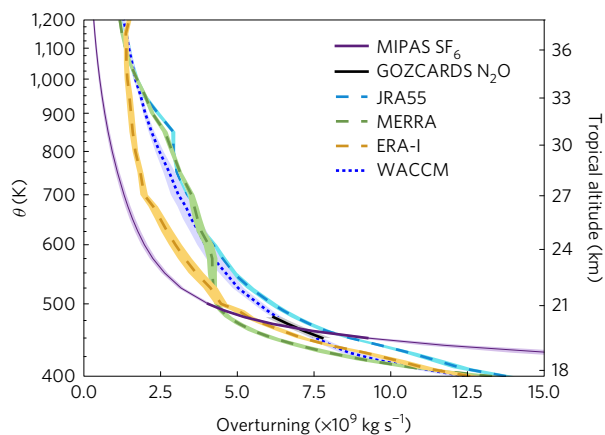


Figure 3 | The strength of the total overturning circulation through each isentrope averaged between 2007–2011. The solid lines are for the data-based estimates MIPAS SF₆ in purple and GOZCARDS N₂O in black. Reanalyses are shown in dashed lines: JRA 55 in light blue, MERRA in green and ERA-Interim in gold. The dotted blue line is WACCM. The shading shows one standard deviation of the five annual averages. The details of the calculation for each data product, the model and the reanalyses are described in the text. The mean height of each isentrope in the tropics (calculated from MIPAS pressure and temperature) is on the right y-axis. Where the line for the MIPAS SF₆-age difference is thinner, we believe there is a bias in either the data or the SF₆ to age conversion (see discussion in Supplementary Information).

These six estimates of the strength of the circulation are quite different, as can be seen by examining the circulation at individual levels. At the lowermost levels, the reanalyses tend to agree, while the MIPAS SF₆-age circulation estimate is much greater because of its very low ΔT . In the range where we have estimates from both observational data sets, they agree closely and are flanked by the reanalyses, which vary more widely (see Supplementary Information for more details). At 500 K and above, the MIPAS SF₆-age-based circulation strength has the lowest value, and at 900 K and above, it is lower by a factor of three. The circulation strength from MIPAS SF₆-age ΔT is biased low, consistent with the sink of SF₆ in the mesosphere²⁴. The disagreement at 1,200 K would require that the bias be nearly 300% for the model and reanalyses to agree with the data. In addition to the disagreement of MIPAS SF₆-age circulation strength with the model and reanalyses, there is significant disagreement between different reanalyses. MERRA has a distinct vertical structure, with weaker circulation in the lower stratosphere and stronger circulation in the mid-stratosphere. JRA 55 and ERA-Interim have a similar vertical structure; JRA 55 is stronger by around $3 \times 10^9 \text{ kg s}^{-1}$, except above 800 K, where it decreases more quickly with potential temperature than ERA-Interim so that they converge by 1,200 K. The shading is the standard deviation of the annual averages that make up the five-year average, and it shows the small interannual variability.

A benchmark and the need for more data

The strength of the stratospheric circulation helps determine transport of stratospheric ozone, stratosphere–troposphere exchange, and the transport of water vapour into the stratosphere³⁷. Stratospheric water vapour has been demonstrated using both data³⁸ and a model³⁹ to impact the tropospheric climate. The stratospheric ozone hole recovery is also influenced by the strength of the circulation⁴⁰.

We have calculated the strength of the overturning circulation of the stratosphere from observations, reanalyses, and a model. We find that at 460 K (about 60 hPa or 20 km in the tropics), the total overturning circulation of the stratosphere is $7.3 \pm 0.3 \times 10^9 \text{ kg s}^{-1}$, based on the agreement of two independent

global satellite data products to within 4% and including interannual variability estimated from WACCM (see Methods). Accounting for the potential high bias induced by the method, this estimate becomes $6.3\text{--}7.6 \times 10^9 \text{ kg s}^{-1}$. Despite this wide range, two of the three reanalysis products lie outside of this range, suggesting deficiencies in their lower stratospheric transport (see Supplementary Table 1). This value can be used as a metric to determine the accuracy of the mean transport of climate models. Because the diabatic circulation and not the residual circulation is used, the computational demands for this metric are minimal, requiring only monthly mean total diabatic heating and temperature on pressure levels.

The global SF₆ data have enabled this quantitative calculation of the diabatic circulation in the middle and upper stratosphere. However, the interpretation of age from SF₆ is limited because we cannot quantify the impact of the mesospheric sink of SF₆, which is important above 550 K. This makes the age difference a minimum of 60% too high at 1,200 K, which would imply a 35% low bias in the overturning strength at 1,200 K, and we cannot estimate an upper bound on the bias. The reanalyses may correctly represent the stratospheric circulation where they agree at the uppermost levels, although the data becomes more limited there⁴¹. Beneath 900 K, however, the reanalyses disagree with each other as well as with the circulation strength implied by data; it is clear that the data assimilated into these reanalyses are not sufficient to constrain estimates of the circulation.

Climate models predict an increase in the strength of the Brewer–Dobson circulation of about 2% per decade^{42,43}, and much effort has recently gone towards calculating trends in the stratospheric circulation based on observations and reanalyses to see if such a trend can be detected^{2,9,44,45}. However, the mean diabatic circulation strength is not known except at one level. At upper levels, the circulation is uncertain to within at least 100%. We suggest cautious interpretation of trends in light of this uncertainty. More global age of air tracer data, in particular CO₂, would provide an independent estimate of age difference and thus the strength of the diabatic stratospheric circulation. High-altitude balloon and aircraft measurements could be very useful; further characterization of compact relationships between age and long-lived tracers, such as N₂O or methane, would provide additional constraints on the circulation in the lower stratosphere by enabling more complete utilization of current global satellite data.

Methods

Methods, including statements of data availability and any associated accession codes and references, are available in the [online version of this paper](#).

Received 22 February 2017; accepted 21 July 2017;
published online 28 August 2017

References

1. Stiller, G. P. *et al.* Observed temporal evolution of global mean age of stratospheric air for the 2002 to 2010 period. *Atmos. Chem. Phys.* **12**, 3311–3331 (2012).
2. Engel, A. *et al.* Age of stratospheric air unchanged within uncertainties over the past 30 years. *Nat. Geosci.* **2**, 28–31 (2009).
3. Mahieu, E. *et al.* Recent Northern Hemisphere stratospheric HCl increase due to atmospheric circulation changes. *Nature* **515**, 104–107 (2014).
4. Haenel, F. J. *et al.* Reassessment of MIPAS age of air trends and variability. *Atmos. Chem. Phys.* **15**, 13161–13176 (2015).
5. Mote, P. W. *et al.* An atmospheric tape recorder: the imprint of tropical tropopause temperatures on stratospheric water vapor. *J. Geophys. Res.* **101**, 3989–4006 (1996).
6. Schoeberl, M. R. *et al.* Comparison of lower stratospheric tropical mean vertical velocities. *J. Geophys. Res.* **113**, D24109 (2008).
7. Flury, T., Wu, D. L. & Read, W. G. Variability in the speed of the Brewer–Dobson circulation as observed by Aura/MLS. *Atmos. Chem. Phys.* **13**, 4563–4575 (2013).

8. Butchart, N. *et al.* Multimodel climate and variability of the stratosphere. *J. Geophys. Res.* **116**, D05102 (2011).
9. Abalos, M., Legras, B., Ploeger, F. & Randel, W. J. Evaluating the advective Brewer–Dobson circulation in three reanalyses for the period 1979–2012. *J. Geophys. Res.* **120**, 7534–7554 (2015).
10. Neu, J. L. & Plumb, R. A. Age of air in a “leaky pipe” model of stratospheric transport. *J. Geophys. Res.* **104**, 19243–19255 (1999).
11. Linz, M., Plumb, R. A., Gerber, E. P. & Sheshadri, A. The relationship between age of air and the diabatic circulation of the stratosphere. *J. Atmos. Sci.* **73**, 4507–4518 (2016).
12. Waugh, D. & Hall, T. M. Age of stratospheric air: theory, observations, and models. *Rev. Geophys.* **40**, 1010 (2002).
13. von Clarmann, T. *et al.* Retrieval of temperature and tangent altitude pointing from limb emission spectra recorded from space by the Michelson Interferometer for Passive Atmospheric Sounding (MIPAS). *J. Geophys. Res.* **108**, 4736 (2003).
14. von Clarmann, T. *et al.* Retrieval of temperature, H₂O, O₃, HNO₃, CH₄, N₂O, ClONO₂ and ClO from MIPAS reduced resolution nominal mode limb emission measurements. *Atmos. Meas. Tech.* **2**, 159–175 (2009).
15. Plumb, R. A. *et al.* Global tracer modeling during SOLVE: high-latitude descent and mixing. *J. Geophys. Res.* **107**, 8309 (2002).
16. Ray, E. A. *et al.* Quantification of the SF₆ lifetime based on mesospheric loss measured in the stratospheric polar vortex. *J. Geophys. Res.* **122**, 4626–4638 (2017).
17. Hall, T. M. & Waugh, D. W. Influence of nonlocal chemistry on tracer distributions: inferring the mean age of air from SF₆. *J. Geophys. Res.* **103**, 13327–13336 (1998).
18. Marsh, D. R. *et al.* Climate Change from 1850 to 2005 simulated in CESM1(WACCM). *J. Clim.* **26**, 7372–7391 (2013).
19. Garcia, R. R., Smith, A. K., Kinnison, D. E., de la Camara, A. & Murphy, D. J. Modification of the gravity wave parameterization in the whole atmosphere community climate model: motivation and results. *J. Atmos. Sci.* **74**, 275–291 (2017).
20. Lin, S. J. A “vertically Lagrangian” finite-volume dynamical core for global models. *Mon. Weath. Rev.* **132**, 2293–2307 (2004).
21. Neale, R. B. *et al.* The mean climate of the Community Atmosphere Model (CAM4) in forced SST and fully coupled experiments. *J. Clim.* **26**, 5150–5168 (2013).
22. Morgenstern, O. *et al.* Review of the global models used within phase 1 of the Chemistry–Climate Model Initiative (CCMI). *Geosci. Model Dev.* **10**, 639–671 (2017).
23. Totterdill, A., Kovács, T., Gomez-Martin, J. C., Feng, W. & Plane, J. M. C. Mesospheric removal of very long-lived greenhouse gases SF₆ and CFC-115 by metal reactions, Lyman- α photolysis, and electron attachment. *J. Phys. Chem. A* **119**, 2016–2025 (2015).
24. Kovács, T. *et al.* Determination of the atmospheric lifetime and global warming potential of sulfur hexafluoride using a three-dimensional model. *Atmos. Chem. Phys.* **17**, 883–898 (2017).
25. Funke, B. *et al.* Composition changes after the “Halloween” solar proton event: the High Energy Particle Precipitation in the Atmosphere (HEPPA) model versus MIPAS data intercomparison study. *Atmos. Chem. Phys.* **11**, 9089–9139 (2011).
26. Funke, B. *et al.* HEPPA-II model–measurement intercomparison project: EPP indirect effects during the dynamically perturbed NH winter 2008–2009. *Atmos. Chem. Phys.* **17**, 3573–3604 (2017).
27. Carlotti, M., Dinelli, B. M., Innocenti, G. & Palchetti, L. A strategy for the measurement of CO₂ distribution in the stratosphere. *Atmos. Meas. Tech.* **9**, 5853–5867 (2016).
28. Plumb, R. A. & Ko, M. K. W. Interrelationships between mixing ratios of long-lived stratospheric constituents. *J. Geophys. Res.* **97**, 10145–10156 (1992).
29. Andrews, A. E. *et al.* Mean ages of stratospheric air derived from *in situ* observations of CO₂, CH₄, and N₂O. *J. Geophys. Res.* **106**, 32295–32314 (2001).
30. Froidevaux, L. *et al.* GOZCARDS Source Data for Nitrous Oxide Monthly Zonal Averages on a Geodetic Latitude and Pressure Grid v1.01 (NASA GESDISC, 2013).
31. Strahan, S. E. *et al.* Using transport diagnostics to understand chemistry climate model ozone simulations. *J. Geophys. Res.* **116**, D17302 (2011).
32. Sparling, L. C. *et al.* Diabatic cross-isentropic dispersion in the lower stratosphere. *J. Geophys. Res.* **102**, 25817–25829 (1997).
33. Birner, T. & Bönisch, H. Residual circulation trajectories and transit times into the extratropical lowermost stratosphere. *Atmos. Chem. Phys.* **11**, 817–827 (2011).
34. Rienecker, M. M. *et al.* MERRA: NASA’s modern-era retrospective analysis for research and applications. *J. Clim.* **24**, 3624–3648 (2011).
35. Kobayashi, S. *et al.* The JRA-55 reanalysis: general specifications and basic characteristics. *J. Meteorol. Soc. Jpn* **93**, 5–48 (2015).
36. Dee, D. P. *et al.* The ERA-Interim reanalysis: configuration and performance of the data assimilation system. *Q. J. R. Meteorol. Soc.* **137**, 553–597 (2011).
37. Butchart, N. The Brewer–Dobson circulation. *Rev. Geophys.* **52**, 157–184 (2014).
38. Solomon, S. *et al.* Contributions of stratospheric water vapor to decadal changes in the rate of global warming. *Science* **327**, 1219–1223 (2010).
39. Dessler, A. E., Schoeberl, M. R., Wang, T., Davis, S. M. & Rosenlof, K. H. Stratospheric water vapor feedback. *Proc. Natl Acad. Sci. USA* **110**, 18087–18091 (2013).
40. Solomon, S. *et al.* Emergence of healing in the Antarctic ozone layer. *Science* **353**, 269–274 (2016).
41. Dee, D. P. & Uppala, S. Variational bias correction of satellite radiance data in the era-interim reanalysis. *Q. J. R. Meteorol. Soc.* **135**, 1830–1841 (2009).
42. Butchart, N. *et al.* Simulations of anthropogenic change in the strength of the Brewer–Dobson circulation. *Clim. Dynam.* **27**, 727–741 (2006).
43. Hardiman, S. C., Butchart, N. & Calvo, N. The morphology of the Brewer–Dobson circulation and its response to climate change in CMIP5 simulations. *Q. J. R. Meteorol. Soc.* **140**, 1958–1965 (2014).
44. Seviour, W. J. M., Butchart, N. & Hardiman, S. C. The Brewer–Dobson circulation inferred from ERA-Interim. *Q. J. R. Meteorol. Soc.* **138**, 878–888 (2012).
45. Diallo, M., Legras, B. & Chédin, A. Age of stratospheric air in the ERA-Interim. *Atmos. Chem. Phys.* **12**, 12133–12154 (2012).
46. *Climate Change Indicators in the United States* (US Environmental Protection Agency, 2016).

Acknowledgements

We thank A. Sheshadri and S. Solomon for helpful discussions. Funding for M.L. was provided by the National Defense Science and Engineering Graduate fellowship. This work was supported in part by the National Science Foundation grant AGS-1547733 to MIT and AGS-1546585 to NYU. F.J.H. was funded by the “CAWSES” priority programme of the German Research Foundation (DFG) under project STI 210/5-3 and by the German Federal Ministry of Education and Research (BMBF) within the “ROMIC” programme under project 01LG1221B. MIPAS data processing was co-funded by the German Federal Ministry of Economics and Technology (BMWi) within the “SEREMISA” project under contract number 50EE1547. A.M. acknowledges funding support from the European Research Council through the ACCI project (Grant 267760) lead by J. Pyle. The National Center for Atmospheric Research (NCAR) is sponsored by the US National Science Foundation. Any opinions, findings, and conclusions or recommendations expressed in the publication are those of the author(s) and do not necessarily reflect the views of the National Science Foundation. WACCM is a component of the Community Earth System Model (CESM), which is supported by the National Science Foundation (NSF) and the Office of Science of the US Department of Energy. Computing resources were provided by NCAR’s Climate Simulation Laboratory, sponsored by NSF and other agencies. This research was enabled by the computational and storage resources of NCAR’s Computational and Information System Laboratory (CISL). A portion of the research was carried out at the Jet Propulsion Laboratory, California Institute of Technology, under a contract with the NASA Aeronautics and Space Administration. One of the datasets used for this study is from the Japanese 55-year Reanalysis (JRA 55) project carried out by the Japan Meteorological Agency (JMA). MERRA was developed by the Global Modeling and Assimilation Office and supported by the NASA Modeling, Analysis and Prediction Program. Source data files can be acquired from the Goddard Earth Science Data Information Services Center (GES DISC). ERA-Interim data provided courtesy of ECMWF.

Author contributions

M.L. performed the research and wrote the manuscript with the guidance of R.A.P. and E.P.G. F.J.H. and G.S. provided the MIPAS age, pressure and temperature data and guidance on that product. D.E.K. provided the WACCM output. A.M. performed calculations with ERA-Interim. J.L.N. provided help with the N₂O data and consulted on the manuscript.

Additional information

Supplementary information is available in the [online version of the paper](#). Reprints and permissions information is available online at www.nature.com/reprints. Publisher’s note: Springer Nature remains neutral with regard to jurisdictional claims in published maps and institutional affiliations. Correspondence and requests for materials should be addressed to M.L.

Competing financial interests

The authors declare no competing financial interests.

Methods

MIPAS SF₆. For more details on validation and methods, we refer the readers to the papers on this product^{1,4,47}. We note that the vertical resolution is 4 to 6 km at 20 km, 7 to 10 km at 30 km, and 12 to 18 km at 40 km altitude. Noise error on individual profiles is of the order of 20%, but because of the many profiles, meaningful SF₆ has been obtained by using monthly and zonal mean averages in 10° bins.

N₂O. An empirical fit between N₂O and age from an extensive record of NASA ER-2 aircraft flights and high-altitude balloons from 1992–1998 has been calculated²⁹. Age is based on CO₂, and for details of the conversion from CO₂ to age, we refer the reader to the original study²⁹. The fit holds well for 50 ppbv < N₂O < 300 ppbv and is given by the equation $F(N_2O) = 0.0581(313 - N_2O) - 0.000254(313 - N_2O)^2 + 4.41 \times 10^{-7}(313 - N_2O)^3$, where 313 ppbv was the average tropospheric mixing ratio for 1992–1998. Although different tracer–tracer relationships are expected in the tropics and the extratropics^{31,48}, the limited tropical data used to calculate this relationship were not treated separately. To account for the increase in tropospheric N₂O, we calculate the trend from the data product provided by the EPA Climate Indicators⁴⁶, a combination of station measurements from Cape Grim, Australia; Mauna Loa, Hawaii; the South Pole; and Barrow, Alaska. The slope is 0.806 ± 0.014 ppbv yr⁻¹. (One standard error on the slope is reported. Using only Mauna Loa, the tropical station, does not change the fit much, since N₂O is fairly well mixed in the troposphere.) We linearly adjust the GOZCARDS N₂O data using this slope to account for the growth in tropospheric N₂O, although simply subtracting the mean difference in tropospheric N₂O between 2009 and 1995 yielded very similar results. Then we apply the empirical relationship between 2004 and 2012 to obtain age estimates. Age difference is calculated only on those levels for which there are very few gaps in age. Only 460 and 470 K have no gaps at all. This method relies on several potentially problematic assumptions: the compact relationship from the 1990s is assumed to be applicable over a decade later; the tropics are assumed to be represented by this relationship well enough to obtain unbiased estimates of age difference; and linearly adjusting the data is assumed to sufficiently account for the changing tropospheric source.

WACCM SF₆. The method to calculate age from SF₆ in WACCM is as follows: the SF₆ on pressure levels is zonally averaged and then averaged in the same latitudinal bins that were used for MIPAS. That zonally averaged SF₆ is then converted to age¹. The reference curve for SF₆ is the zonal mean value in the tropics at 100 hPa just

north of the equator (0.5° N) with a one-year low-pass fourth-order Butterworth filter applied to remove the weak seasonal cycle. Results are insensitive to the filtering provided the filter is sufficient to obtain a strictly increasing reference curve. We use the same method for correcting the age of air for the nonlinear tropospheric growth, with a Newtonian iteration (see ref. 1 equation 3). The nonlinearity correction is insensitive to the choice of constant parameter used to describe the relationship of the width of the age spectrum with the age. Once the age is determined, it is interpolated to isentropic levels using zonal mean temperatures that have also been binned by latitude according to the MIPAS grid. No attempt is made in this work to adjust the age for the mesospheric sink.

Statistics for 460 K overturning. To calculate the average overturning circulation strength where the two data estimates agree most closely (within 5% at 460 K), we average them. The error estimate is based on the variability in the total overturning circulation strength from WACCM calculated using SF₆ age to infer the circulation (M/SF₆-age ΔT). We take the average of five annual averages chosen randomly from the annual averages from 1999–2014 100,000 times. The standard deviation of the 100,000 resulting mean circulation strength estimates (0.14×10^9 kg s⁻¹) is taken to be half of the error. We repeated this procedure using the true overturning circulation strength (\mathcal{M}) and found smaller variations in the standard deviation (0.09×10^9 kg s⁻¹). This error estimate assumes that WACCM represents the variability of the true circulation. The standard deviations of the five annual averages that were averaged for each data estimate were considerably smaller than these reported error bars. We therefore believe this is a conservative representation of the uncertainty in the diabatic circulation strength.

Code availability. Codes used to generate the primary figures in this article is available at https://figshare.com/articles/NGeo2017_plots_m/5229844/1, and any additional code can be obtained from the corresponding author upon request.

Data availability. The data for the primary figures in this article are available at https://figshare.com/articles/NGeo2017_plots_m/5229844/1, and any additional data can be obtained from the corresponding author upon request.

References

47. Stiller, G. P. *et al.* Global distribution of mean age of stratospheric air from MIPAS SF₆ measurements. *Atmos. Chem. Phys.* **8**, 677–695 (2008).
48. Plumb, R. A. Tracer interrelationships in the stratosphere. *Rev. Geophys.* **45**, RG4005 (2007).